A novel interpenetrated anion-pillared porous material with high water tolerance afforded efficient C_2H_2/C_2H_4 separation

Lifeng Yang,[a] Anye Jin, [a] Lisha Ge,[a] Xili Cui,[a] Huabin Xing*[a]

[a] Key Laboratory of Biomass Chemical Engineering of Ministry of Education, College of Chemical and Biological Engineering, Zhejiang University, Hangzhou 310027

Supplementary Information

Table of contents

Methods and Characterization

Synthesis of ZU-62-Ni

The water solution (4.0 mL) of $NiNbOF_5$ (0.0730 g) and the methanol solution (4.0mL) of 4, 4'-bipyridylacetylene (0.0515 g).were preheated for 10 min at 338 K. Then the water solution was slowly dropped in to the methanol solution to afford the milk white solution. The mixture was heated at 358 K for 24 h. The bulk synthesis using the 5 times more raw materials was conducted in the same procedure, except the usage of both the water and methanol was increased to 20 mL and the reaction time was extended to 48 h. The obtained white powder was exchanged with methanol for one day. 2 mL of H_2O: CH_3OH (v/v=1:1) was layered over 3 mL methanol solution containing 4, 4'-bipyridylacetylene (0.073g in 10 mL CH_3OH) in a long thin tube. 3 mL $NiNbOF_5$ (0.05 g in 10 mL H_2O) was carefully layered over the buffer layer. The tube was sealed and left undisturbed at 298 K. After 1 week, white crystal was obtained.

Single Crystal X-ray diffraction data for ZU-62-Ni

Crystal data for ZU-62-Ni was collected at 123(2) K on a BrukerAXS D8 VENTURE diffractometer equipped with a PHOTON-100/CMOS detector (CuKα, λ = 1.5418 Å). Indexing was performed using APEX2. Data integration and reduction were completed using SaintPlus 6.01. Absorption correction was performed by the multi-scan method implemented in SADABS. The space group was determined using XPREP implemented in APEX2.1 The structure was solved with SHELXL-2018/3 (direct methods) and refined on F2 (nonlinear least-squares method) with SHELXL-2018/3 contained in APEX2, WinGX v1.70.01, and OLEX2 v1.1.5 program packages. All non-hydrogen atoms were refined anisotropically. The contribution of disordered solvent molecules was treated as diffuse using the Squeeze routine implemented in Platon. Powder X-ray diffraction (PXRD) was carried out at room temperature on a Bruker D8 Advance θ/θ diffractometer using Cu-Kα radiation (λ=1.5418 Å). The crystal data was summarized in Table S1.

The residual electron densities in the solvent-accessible void due to disordered solvent molecules were treated with the PlATON SQUEEZE program. And according to the electron densities as well as the used solvent, the residual solvents were assumed to be one CH_3OH and three H_2O, however, the actual location of the solvent was unable to be determined due to its serious disorder. The proper formula was assumed to be $Ni(dpa)_2(NbOF_5)\cdot 1CH_3OH\cdot 3H_2O$.

Characterization Methods

Powder X-ray diffraction (PXRD) data was collected on a SHIMADZU XRD-6000 diffractometer (Cu $K_\alpha\lambda$ = 1.540598 Å) with an operating power of 40 KV, 30mA and a scan speed of 4.0°/min. The range of 2θ was from 5° to 60°. The thermal gravimetric analysis was performed on an instrument of TGA Q500 V20.13 Build 39. Experiments were carried out using a platinum pan under nitrogen atmosphere. Firstly，the sample was removed water at 80°C and equilibrated for 5 minutes, then cooled down to 50°C. The data were collected at the temperature range of 50°C to 600 °C with a ramp of 10°C min^{-1}.

Gas Adsorption Measurements and breakthrough experiment

The measurements of C_2H_2 and C_2H_4 adsorption isotherms were performed on the Micrometrics

ASAP 2460. Before gas adsorption measurements, 100-200 mg sample of ZU-62-Ni were degassed at 80 ^{0}C for 24 hours until the pressure dropped below 50 μmHg. The sorption isotherms were collected at 273~313 K on activated samples.

Breakthrough experiment was carried out in a 4.6 mm inner diameter column of 50 mm length packed with 0.30 g of ZU-62-Ni. The column was first activated at 80 ^{0}C under 10 mL flow of He for 24 hours. The mixed gas of C_2H_2/C_2H_4= 1/99 (v/v) was then introduced at 1.5 mL min^{-1}. Outlet gas from the column was monitored using gas chromatography (GC-2010 plus) with the flame ionization detector (FID). After the breakthrough experiment, the sample was regenerated with He flow 15 mL min^{-1} under 25 °C for 8 hours.

Virial Equation: Estimation of the isoteric heates of gas adsorption (Qst)

A virial-type equation of comprising the temperature-independent parameters $\mathbf{a_i}$ and $\mathbf{b_j}$ are employed to calculate the isosteric heat for C_2H_2 (at 273 K, 298 K and 313 K). The adsorption isotherm data are fitted using the following equation:

$$ln\,P = ln\,N + 1/T\sum_{i=0}^{m} aiNi + \sum_{j=0}^{n} bjNj \qquad (1)$$

Here, ***P*** is the pressure expressed in **mmHg**, ***N*** is the amount adsorbed in **mg g^{-1}**, T is the temperature in K, $\boldsymbol{a_i}$ and $\boldsymbol{b_j}$ are virial coefficients, and **m, n** represent the number of coefficients reuquired to adequately describe the isotherms. The values of the virial coefficients $\mathbf{a_0}$ to $\mathbf{a_m}$ are then used to calcualte the C_2H_2 isosteric heat of adsorption using the following equation:

$$Qst = -R\sum_{i=0}^{m} aiNi \qquad (2)$$

Q_{st} is the gas coverage-dependent isosteric heat of adsorption and R is the universal gas constant.

Fitting of Pure Component Isotherms

The adsorption isotherms of C_2H_2 and C_2H_4 in ZU-62-Ni were fitted using a dual-site Langmuir-Freundlich model.

$$q = q_{A,sat}\frac{b_A p^{v_A}}{1+b_A p^{v_A}} + q_{B,sat}\frac{b_B p^{v_B}}{1+b_B p^{v_B}} \qquad (3)$$

Here, *P* is the pressure of the bulk gas at equilibrium with the adsorbed phase (kPa), *q* is the adsorbed amount per mass of adsorbent (mol kg^{-1}), $q_{A,sat}$ an $q_{B,sat}$ are the saturation capacities of site1 and 2 (mol kg^{-1}), b_A and b_B are the affinity coefficients of site 1 and 2 (kPa^{-1}), and v_A and v_B represent the deviations from an ideal homogeneous surface.

The C_2H_2 isosteric heat of adsorption within ZU-62-Ni, Q_{st}, defined as:

$$Q_{st} = RT^2\left(\frac{\partial \ln p}{\partial T}\right)_q \qquad (4)$$

The calculations are based on the use of the Clausius-Clapeyron equation.

IAST Calculations of Adsorption Selectivities.

The adsorption selectivity for C_2H_2/C_2H_4 separation was defined by [4]

$$S_{ads} = \frac{q_1 / q_2}{p_1 / p_2} \tag{5}$$

q_1, and q_2 are the molar loadings in the adsorbed phase in equilibrium with the bulk gas phase with partial pressures p_1, and p_2.

Table S1. Crystal structure data of ZU-62-Ni.

Unit cell parameters	
Formula sum	C24 H16 F5 N4 Nb Ni O
Formula weight	623.03 g/mol
Crystal system	tetragonal
Space –group	I 4/m m m (139)
Cell parameters	a=13.8526(6) Å c=7.8862(4) Å
Cell ratio	a/b=1.0000 b/c=1.7566 c/a=0.5693
Cell volume	1513.32(15) $Å^3$
Z	2
Calc.density	1.3672 g/cm^3

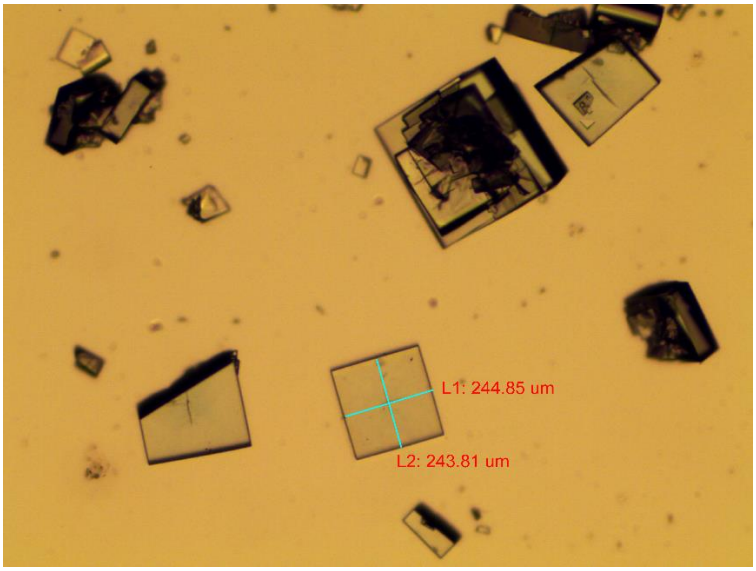

Figure S1. The morphology and size of the as-synthesized ZU-62-Ni crystal.

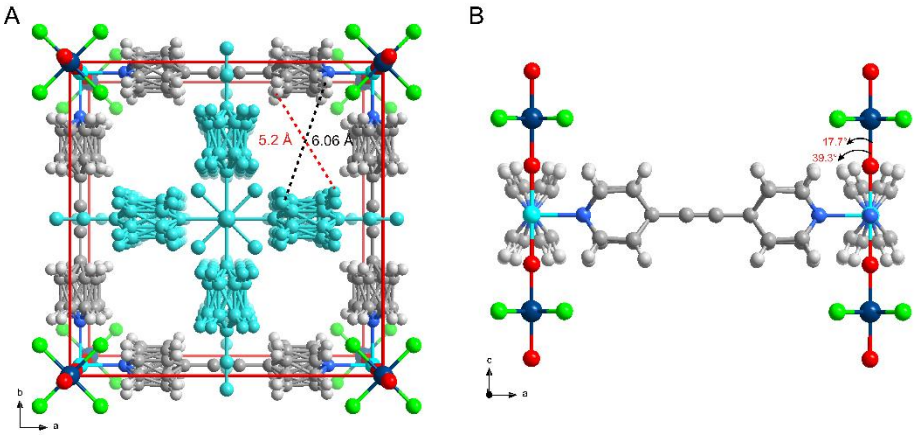

Figure S2: The crystal structure of ZU-62-Ni without solvent.

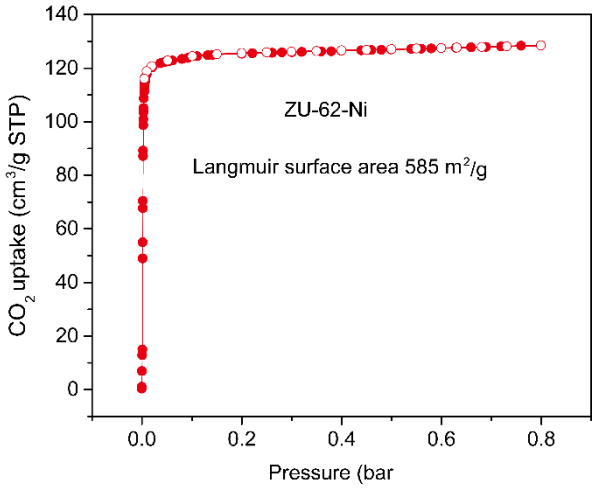

Figure S3:The CO_2 adsorption isotherm on ZU-62-Ni at 196 K.

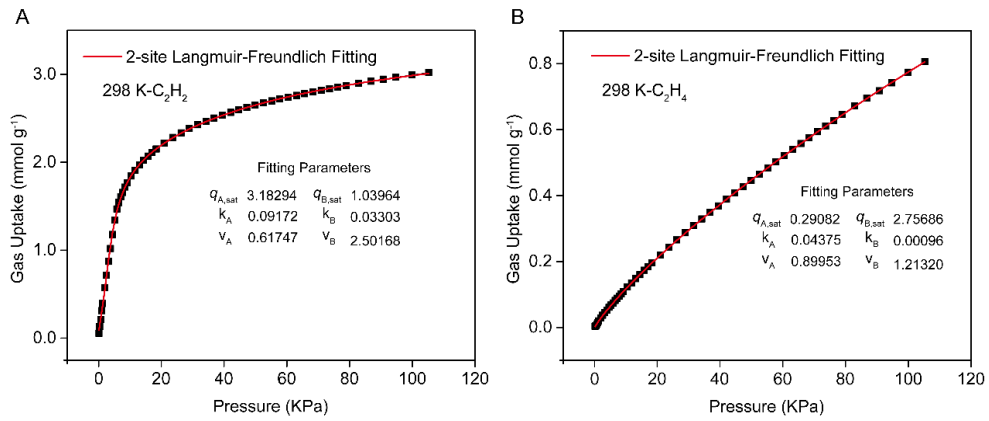

Figure S4: The Langmuir-Freundlich fitting of C_2H_2 and C_2H_4 adsorption isotherms of ZU-62-Ni.

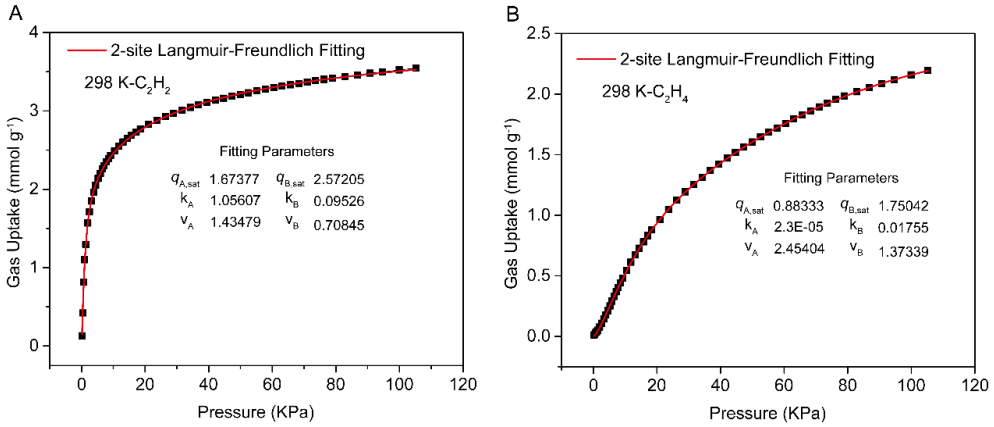

Figure S5: The Langmuir-Freundlich fitting of C_2H_2 and C_2H_4 adsorption isotherms of ZU-62.

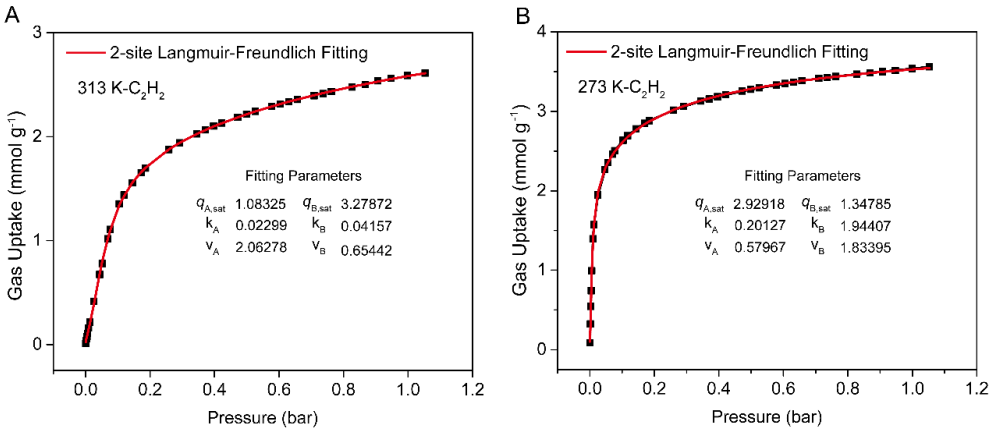

Figure S6: The Langmuir-Freundlich fitting of 273 K and 313 K C_2H_2 adsorption isotherms of ZU-62-Ni.

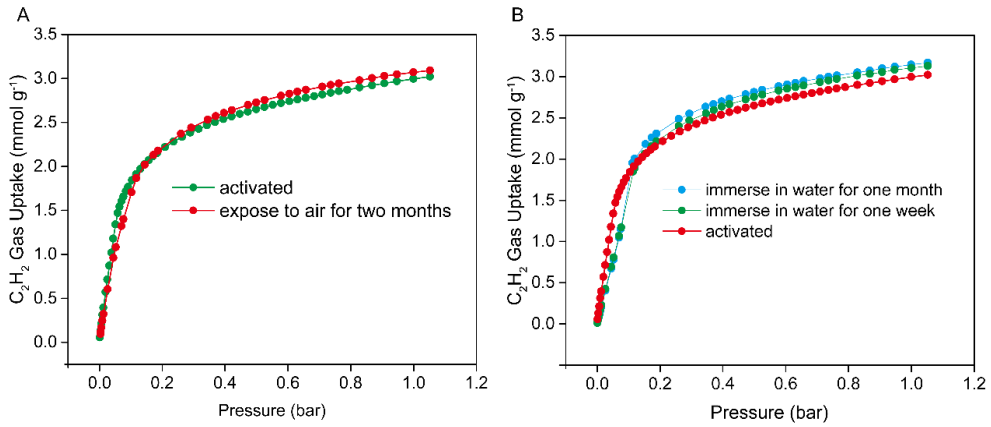

Figure S7: The stability test of ZU-62-Ni to air and water.

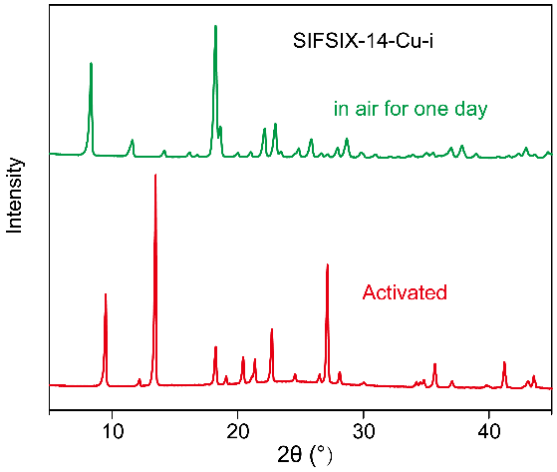

Figure S8: The XRD pattern of SIFSIX-14-Cu-i.

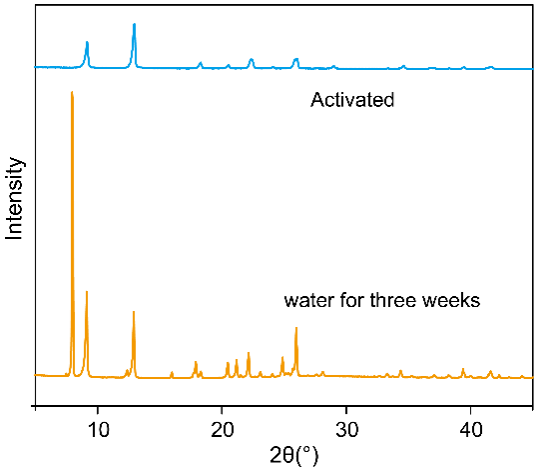

Figure S9: The XRD pattern of SIFSIX-2-Cu-i.

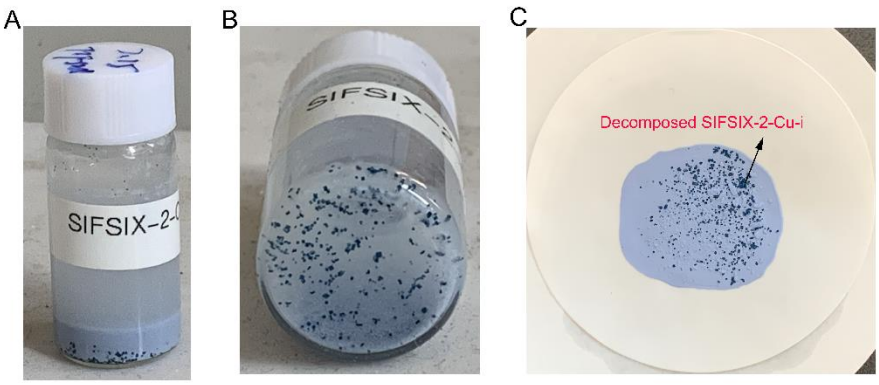

Figure S10: The status of SIFSIX-2-Cu-i after exposed to water for 3 weeks

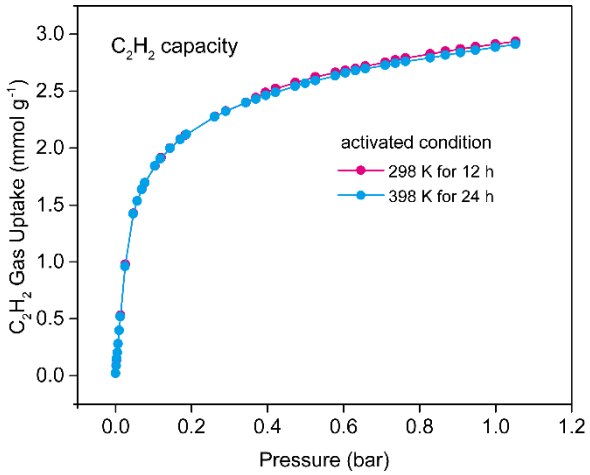

Figure S11: The C_2H_2 capacity of ZU-62-Ni under different activated conditions.

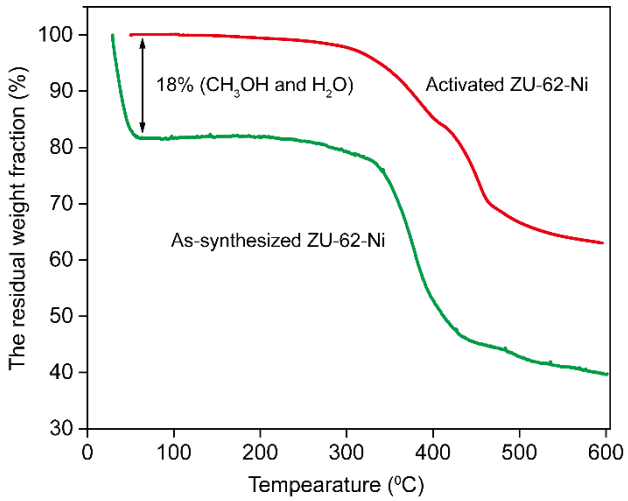

Figure S12: The TGA curve of activated ZU-62-Ni and the as-synthesized ZU-62-Ni.

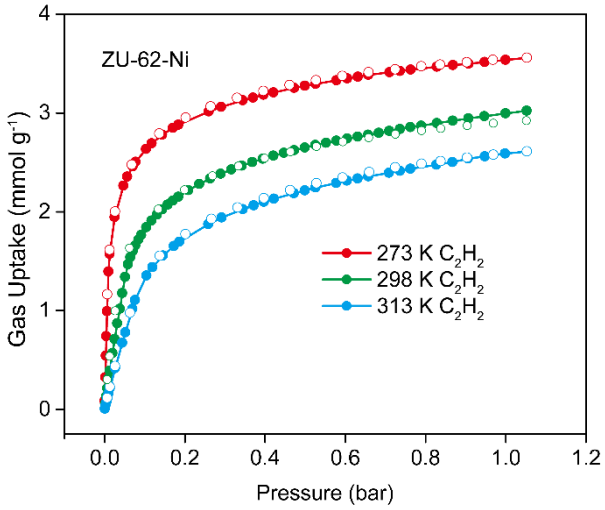

Figure S13: The C_2H_2 adsorption isotherm results of ZU-62-Ni from 273 K to 313 K.

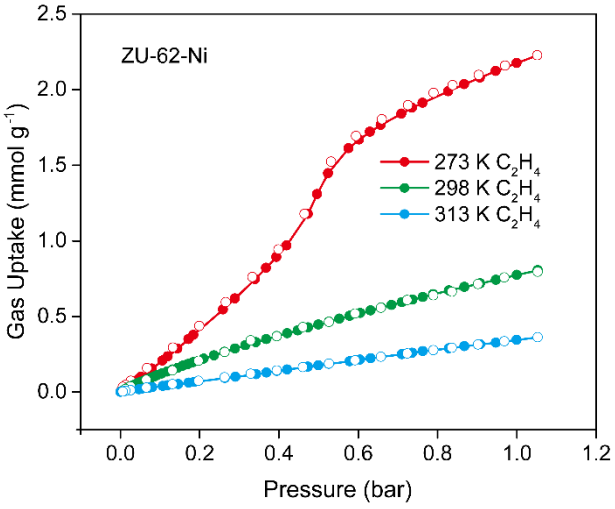

Figure S14: The C_2H_4 adsorption isotherm results of ZU-62-Ni from 273 K to 313 K.

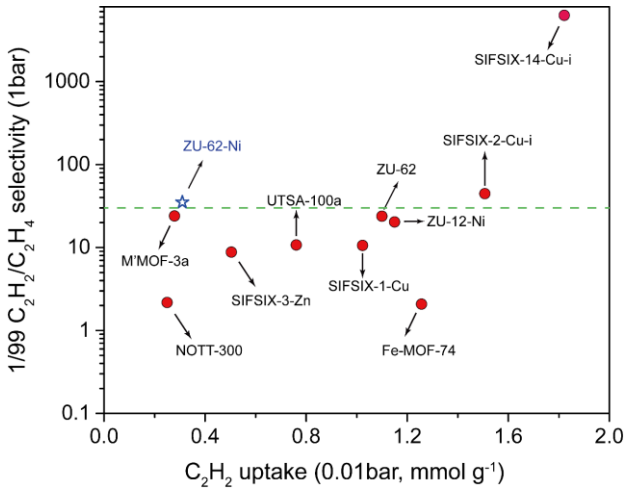

Figure S15: Comparison of C_2H_2/C_2H_4 (1/99) selectivity and C_2H_2 (0.01 bar) uptake of previously reported materials.

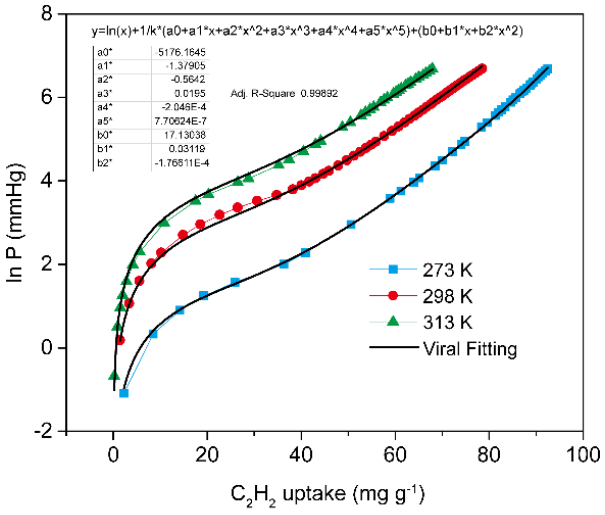

Figure S16: The virial fitting of the C_2H_2 adsorption isotherms for ZU-62-Ni at 273 K, 298 K and 313 K.

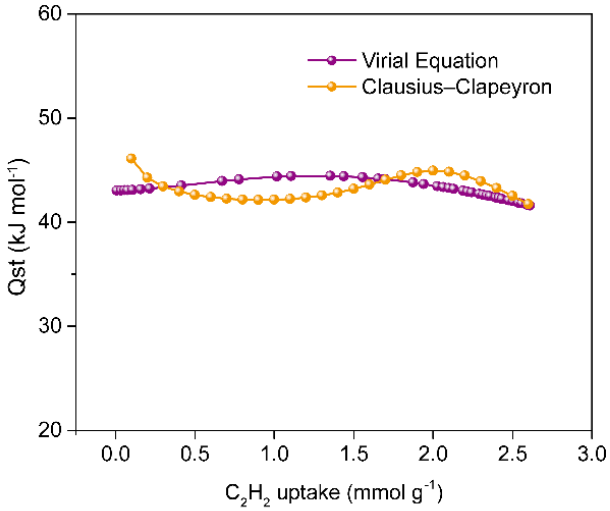

Figure S17: The C_2H_2 isosteric adsorption heat within ZU-62-Ni.

Table S2: The comparison of C_2H_2 and C_2H_4 uptake from gas adsorption isotherms for various materials.

Materials	BET[%] (m^2 g^{-1})	C_2H_2 uptake at 0.01bar (mmol g^{-1})	C_2H_2 uptake at 1bar (mmol g^{-1})	C_2H_4 uptake at 1bar (mmol g^{-1})	C_2H_2/C_2H_4 (1/99) selectivity	Reference
ZU-62-Ni	404†	0.3	3.01	0.8	37.2	This work
ZU-62	476	1.1	3.53	2.19	24	1
ZU-32	467	1.54	3.96	2.19	67	2
ZU-33	424†	1.94	3.78	0.70	1100[&]	2
ZU-12-Ni	480	1.15	4.21	2.42	22.7	3
SIFSIX-2-Cu-i	503	1.5	4.02	2.19	44.54	4
SIFSIX-14-Cu-i	612†	1.82	3.65	0.63	6320[&]	5
SIFSIX-3-Ni	368	0.23	3.30	1.75	5.03	6
SIFSIX-3-Zn	250	0.50	3.64	2.24	8.82	4
SIFSIX-1-Cu	1178	1.02	8.5	4.11	10.63	4
TIFSIX-4-Cu-i	542	0.45	4.3	1.5	11	7
TIFSIX-2-Cu-i	685	1.7	4.1	2.5	55	7
M'MOF-3a	110	0.28	1.9	0.4	24	8
UTSA-100a	970	0.76	4.27	1.66	10.72	9
NOTT-300	1370	0.25	6.34#	4.28#	2.17	10
Fe-MOF-74	1350	1.26	6.8*	6.1*	2.08	11
NKMOF-1-Ni	380	1.69	2.72	2.09	1272.6	12

% BET surface area calculated from N_2 isotherms at 77K.

* at temperature of 318 K.

at temperature of 293 K.

& only for the qualitative comparison

† BET surface area calculated from CO_2 isotherms at 196 K.

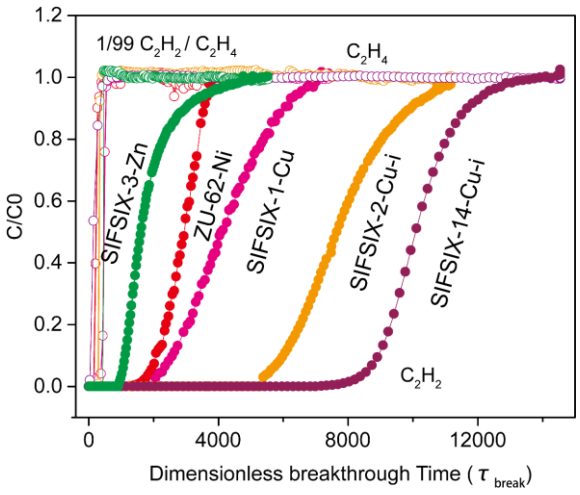

Figure S18: The experimental breakthrough performance of previously reported best-performing materials.

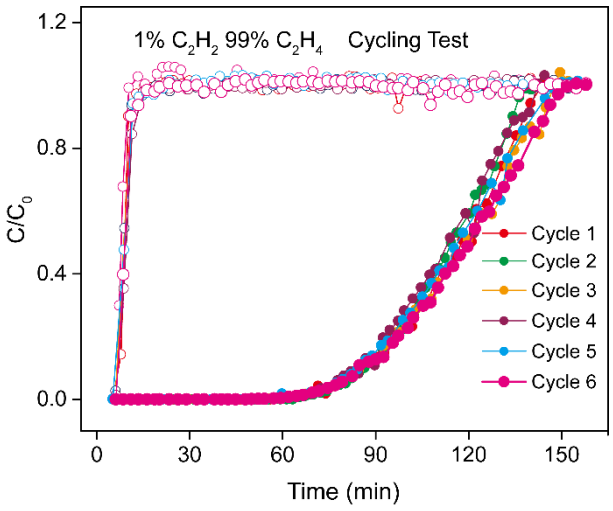

Figure S19: The cycling C_2H_2 / C_2H_4 breakthrough performance. (desorption condition: He flow 15 mL min^{-1} under 25 °C for 8 hours)

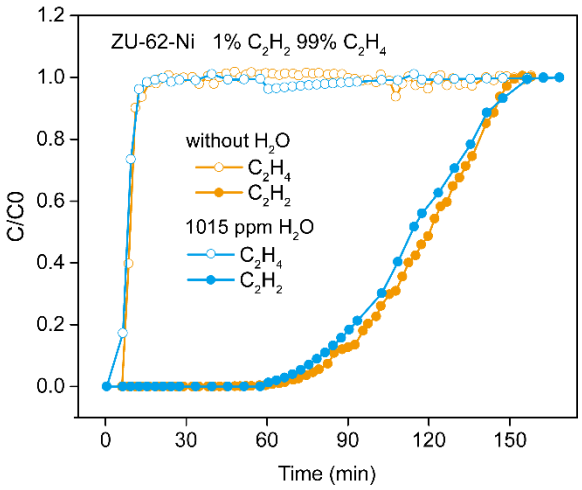

Figure S20: The experimental column breakthrough curves for C_2H_2/C_2H_4 (1/99, v/v) and $C_2H_2/C_2H_4/H_2O$ separations (1.01/98.9, v/v ; with 1015 ppm H_2O) on ZU-62-Ni.

Reference

1. L. F. Yang, X. L. Cui, Z. Q. Zhang, Q. W. Yang, Z. B. Bao, Q. L. Ren and H. B. Xing, Angew. Chem. Int. Ed, 2018, **57**, 13145-13149.
2. Z. Zhang, X. Cui, L. Yang, J. Cui, Z. Bao, Q. Yang and H. Xing, *Ind. Eng. Chem. Res*, 2018, **57**, 7266-7274.
3. M. Jiang, X. Cui, L. Yang, Q. Yang, Z. Zhang, Y. Yang and H. Xing, *Chem. Eng. J*, 2018, **352**, 803-810.
4. X. Cui, K. Chen, H. Xing, Q. Yang, R. Krishna, Z. Bao, H. Wu, W. Zhou, X. Dong, Y. Han, B. Li, Q. Ren, M. J. Zaworotko and B. Chen, Science, 2016, **353**, 141-144.
5. B. Li, X. Cui, D. O'Nolan, H. M. Wen, M. Jiang, R. Krishna, H. Wu, R. B. Lin, Y. S. Chen, D. Yuan, H. Xing, W. Zhou, Q. Ren, G. Qian, M. J. Zaworotko and B. Chen, Adv Mater, 2017, **29**,1704210-1704217.
6. L. Yang, X. Cui, Q. Yang, S. Qian, H. Wu, Z. Bao, Z. Zhang, Q. Ren, W. Zhou, B. Chen and H. Xing, Adv Mater, 2018, **30**, 1705374-1705382.
7. A. Bajpai, D. O'Nolan, D. G. Madden, K. J. Chen, T. Pham, A. Kumar, M. Lusi, J. J. Perry, B. Space and M. J. Zaworotko, *Chem. Commun*, 2017, **53**, 11592-11595.
8. S. C. Xiang, Z. Zhang, C. G. Zhao, K. Hong, X. Zhao, D. R. Ding, M. H. Xie, C. D. Wu, M. C. Das, R. Gill, K. M. Thomas and B. Chen, Nat. Commun, 2011, **2**, 204-211.
9. T. L. Hu, H. Wang, B. Li, R. Krishna, H. Wu, W. Zhou, Y. Zhao, Y. Han, X. Wang, W. Zhu, Z. Yao, S. Xiang and B. Chen, Nat. Commun, 2015, **6**, 7328-7337.
10. S. Yang, A. J. Ramirez-Cuesta, R. Newby, V. Garcia-Sakai, P. Manuel, S. K. Callear, S. I. Campbell, C. C. Tang and M. Schroder, Nat. Chem, 2014, **7**, 121-129.
11. E. D. Bloch, W. L. Queen, R. Krishna, J. M. Zadrozny, C. M. Brown and J. R. Long, Science, 2012, **335**, 1606-1610.
12. Y. L. Peng, T. Pham, P. Li, T. Wang, Y. Chen, K. J. Chen, B. Space, K. Forrest, P. Cheng, Z. Zhang and M. Zaworotko, Angew. Chem. Int. Ed, 2018, **57**, 10971-10975.